Dissection of light-induced charge accumulation at a highly active iron porphyrin: insights in the photocatalytic CO_2 reduction

Eva Pugliese, Philipp Gotico, Iris Wehrung, Bernard Boitrel, Annamaria Quaranta, Minh-Huong Ha-Thi, Thomas Pino, M. Sircoglou, Winfried Leibl, Zakaria Halime, et al.

▶ **To cite this version:**

Eva Pugliese, Philipp Gotico, Iris Wehrung, Bernard Boitrel, Annamaria Quaranta, et al.. Dissection of light-induced charge accumulation at a highly active iron porphyrin: insights in the photocatalytic CO_2 reduction. Angewandte Chemie International Edition, 2022, 61 (14), pp.e202117530. 10.1002/anie.202117530 . hal-03594100

HAL Id: hal-03594100
https://hal.science/hal-03594100v1

Submitted on 11 Apr 2022

HAL is a multi-disciplinary open access archive for the deposit and dissemination of scientific research documents, whether they are published or not. The documents may come from teaching and research institutions in France or abroad, or from public or private research centers.

L'archive ouverte pluridisciplinaire **HAL**, est destinée au dépôt et à la diffusion de documents scientifiques de niveau recherche, publiés ou non, émanant des établissements d'enseignement et de recherche français ou étrangers, des laboratoires publics ou privés.

Distributed under a Creative Commons Attribution - NonCommercial 4.0 International License

Dissection of Light-Induced Charge Accumulation at a Highly Active Iron Porphyrin: Insights in the Photocatalytic CO_2 Reduction

Eva Pugliese,[a] Philipp Gotico,[b] Iris Wehrung,[a] Bernard Boitrel,[c] Annamaria Quaranta,[d] Minh-Huong Ha-Thi,[b] Thomas Pino,[b] Marie Sircoglou,[a] Winfried Leibl,[d] Zakaria Halime,*[a] Ally Aukauloo,*[a,d]

[a] E. Pugliese, I. Wehrung, Dr. M. Sircoglou, Dr. Z. Halime, Prof. A. Aukauloo
Université Paris-Saclay, CNRS, Institut de chimie moléculaire et des matériaux d'Orsay, 91405, Orsay, France.
E-mail: zakaria.halime@universite-paris-saclay.fr, ally.aukauloo@universite-paris-saclay.fr
[b] Dr. Philipp Gotico, Dr. M-H Ha-Thi, Dr. T. Pino
Université Paris-Saclay, CNRS, Institut des Sciences Moléculaires d'Orsay (ISMO), 91405, Orsay, France.
[c] Dr. B. Boitrel
Institut des Sciences Chimiques de Rennes (ISCR)
Université Rennes 1, 35042 Rennes (France)
[d] Dr. A. Quaranta, Dr. W. Leibl, Prof. A. Aukauloo
Institute for Integrative Biology of the Cell (I2BC), CEA, CNRS, Université Paris-Saclay, 91198, Gif-sur-Yvette, France.

Supporting information for this article is given via a link at the end of the document.

Abstract: Iron porphyrins are among the best molecular catalysts for the electrocatalytic CO_2 reduction reaction. Powering these catalysts with the help of photosensitizers comes along with a couple of unsolved challenges that need to be addressed with much vigor. We have designed an iron porphyrin catalyst decorated with urea functions (**UrFe**) acting as a multipoint hydrogen bonding scaffold towards the CO_2 substrate. We found a spectacular photocatalytic activity reaching unreported TONs and TOFs as high as 7270 and 3720 h^{-1} respectively are observed. While the Fe^0 redox state has been widely accepted as the catalytically active species, we show here that the Fe^I species is already involved in the CO_2 activation which represents the rate determining step in the photocatalytic cycle. The urea functions help to dock the CO_2 upon photocatalysis. DFT calculations bring support to our experimental findings that constitute a new paradigm in the catalytic reduction of CO_2.

A remarkable lesson from the functioning of the natural photosynthetic apparatus concerns the coupling of light-triggered single-electron transfer events to multielectron catalysis.[1-2] In the actual context of finding ways to use solar energy to convert H_2O and CO_2 to a renewable energetic vector, chemists want to realize such photo-driven processes in bioinspired synthetic models to understand and optimize the photocatalytic pattern.[3] This research also intersects with the strongly growing field of semi-conductors that sets new opportunities for the design of hybrid systems that can capture light to drive these multi-electron redox processes in a tandem fashion.[4-13] However, the current strategy follows the optimization of each constitutive basic reaction i.e. photooxidation of water and photoreduction of CO_2 or protons separately before conjugating both systems.

The search for molecular catalysts that can realize the activation and selective reduction of CO_2 is monopolizing the attention of many chemists.[14-22] Recent findings in this field are prodigious for the electrocatalytic reduction of CO_2 to various reduced forms of CO_2.[20-28] However, coupling these catalysts with a photoredox module to power the catalysis still faces challenging issues such as deleterious photochemical events leading to poor quantum yields. The specific identification and tracking of both short- and long-lived transient species formed by photoinitiated electron transfer are fundamental to determine the mechanistic routes by which charge shifts, charge accumulation, and catalytic events proceed within the photocatalysis context. Although much more complex, these studies are essential to provide the whole panorama of the critical steps in the photocatalytic cycle. Indeed, knowledge of the limiting and other detrimental steps should help chemists to bypass and ameliorate the energy efficiency of the photocatalytic process. The general photocatalytic scheme of photoreduction of CO_2 by molecular catalysts includes a photosensitizer and a sacrificial electron donor (SED).[29] In absence of a photosensitizer, Bonin-Robert and coll. have investigated the photocatalytic reduction of CO_2 to CO with modified iron porphyrins holding phenolic groups in ortho positions reported as being among the most electroactive catalysts in the literature.[30-31] Their findings clearly demonstrated a more intricate multi-branched mechanistic route in contrast to the

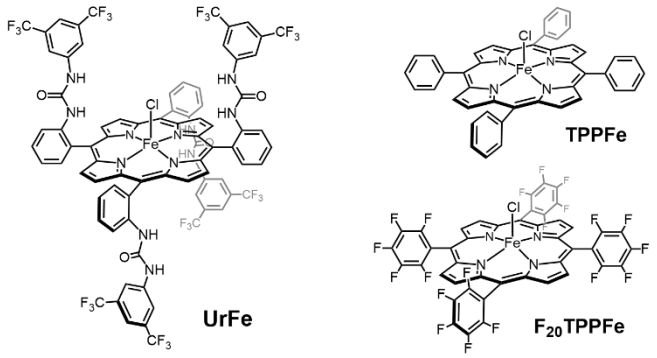

Scheme 1. Molecular representation of catalyst **UrFe** and reference compounds **TPPFe** and **F_{20}TPPFe**.

Table 1. Photocatalysis experiments performed with 20 μM catalyst, 1 mM $Ru(bpy)_3^{2+}$, BIH as SED in DMF/H_2O 9:1 under LED irradiation (100 W m^{-2}) for 2h.

	Catalyst	[Catalyst] (μM)	[SED] (mM)	LED type	CO (μmol)	H_2 (μmol)	Selectivity (CO %)	TON_{CO}	TOF_{CO} (h^{-1})
1	**UrFe**	20	50	White	242	0	100	1865	580
2	**TPPFe**	20	50	White	3	6	34	25	5
3	**F_{20}TPPFe**	20	50	White	19	3	85	143	32
4	**UrFe**	20	50	Blue	395	0.3	99	3036	3141
5	**TPPFe**	20	50	Blue	3	0.7	81	25	5
6	**F_{20}TPPFe**	20	50	Blue	22	12	65	170	78
7	**UrFe**	20	250	Blue	945	3	99	7271	3720
8	**UrFe**	0.2	250	Blue	17	3	86	13299	1160

electrochemical activity. Importantly, the authors have captured the spectroscopic signature of an Fe^{I} intermediate while the putative active Fe^{0} species formed under irradiation was still elusive. Importantly, we have to draw the attention of the reader to early and recent reports suggest that the Fe(I) and Fe(0) oxidation states are better formulated respectively as [Fe^{II}porph$^{\bullet-}$] and [Fe^{II}porph$^{\bullet\bullet 2-}$] metalloradical species. Indeed, after the first metal centered reduction of the starting Fe(III) complex to reach an Fe(II) oxidation state, the porphyrin core acts as the locus for the addition of the two supplementary electrons (porph = porphyrin).[32-35] However, the formal Fe^{I} and Fe^{0} formulations continue to be commonly used for simplicity and we do so herein guardedly.[36] In this study, we pursue a profound investigation on the light-driven CO_2 to CO conversion featuring a modified iron(III)-porphyrin catalyst (shorthanded as **UrFe**) bearing urea functions in the second coordination sphere as multipoint hydrogen-bond pillars (Chart 1). The motivation behind the choice of **UrFe** as catalytic module, was guided by our electrocatalytic study,[37-38] where we have demonstrated that hydrogen-bond interactions induced by these urea groups are involved in different steps of the reaction mechanism such as CO_2 capture and proton transfer from water as proton source, leading to a significant enhancement of catalysis. In combination with $[Ru(bpy)_3]^{2+}$ (bpy = 2,2'-bipyridine) as the photosensitizer and 1,3-dimethyl-2-phenyl-2,3-dihydro-1*H*-benzo[*d*]imidazole (BIH) as a sacrificial electron donor, we found here an exceptional photocatalytic performance of **UrFe** in DMF/H_2O under visible light-irradiation. CO_2 is indeed converted with remarkable turnover numbers (7270) and turnover frequencies (3720 h^{-1}). We have spectroscopically identified the different photo-reduced Fe^{II}, Fe^{I} and Fe^{0} states of the **UrFe** catalyst and compared them to those obtained from electrochemical studies. Importantly, we found that the Fe^{I} state is already interacting with CO_2 during the electrochemical activation and unexpectedly is the steady state during the photocatalytic cycle. We discuss below the role of the urea groups in the stabilization of this unique intermediate that can explain the excellent catalytic reactivity.

In a typical run of the photocatalytic reaction, a DMF/H_2O 9:1 solution containing **UrFe** (20 μM), BIH (50 mM) and $[Ru(bpy)_3]^{2+}$ (1 mM) was irradiated by a white LED source (λ> 405 nm; 100 W m^{-2}) in CO_2 saturated solution. Under these conditions, CO was the only detected reduced product with a TON of 1865 after 200 min of irradiation and a TOF = 580 h^{-1} (Table 1, entry 1 and Figure 1). To evaluate the role of the second coordination sphere in **UrFe**, we performed the photocatalytic experiments with **TPPFe** (iron-tetraphenylporphyrin), the bare parent catalyst as well as its perfluorinated analogue (**F_{20}TPPFe**) having similar redox potentials as **UrFe** (Chart 1, Table S1, Figure 1a and Table 1, entries 2, 3). After similar irradiation time, marked differences in TONs and TOFs were observed for both **TPPFe** (TON = 25, TOF = 5 h^{-1}) and **F_{20}TPPFe** (TON = 143, TOF = 32 h^{-1}). The lower performance of the **TPPFe** may be ascribed to the unfavorable energetics for $Fe^{I/0}$ reduction by the photoredox module (see potentials in table S1). On the other hand, the thermodynamic driving force for the photoreduction of **F_{20}TPPFe^{I}** and **UrFe^{I}** is similar (Table S1). The outperformance of **UrFe** compared to **F_{20}TPPFe** thus clearly suggests a consequential role of the urea functions. We further sought to improve the overall reaction rate by replacing the white light source (λ_{em} > 405 nm, 100 W m^{-2}) used initially by a blue light LED (λ_{em} = 460 nm, 100 W m^{-2}) that leads to a more selective excitation of the MLCT band of the $[Ru(bpy)_3]^{2+}$ photosensitizer (λ_{max} = 454 nm). A substantial improvement in the reaction rate was evidenced (Figure S2) that concurs with the more efficient light capture and electron transfer processes to activate the **UrFe** catalyst. In addition to the improvement of the TOF from 580 h^{-1} to 3141 h^{-1}, the TON also bounced from 1865 to 3036, a value that corresponds to the consumption of the total amount of the sacrificial electron donor (n(BIH) = 325 μmol) initially present in the reaction mixture. Further addition of 200 μmol of BIH to the system led to the production of quasi-stoichiometric amount of CO confirming that BIH was the limiting reagent of the reaction (Figure S3). A

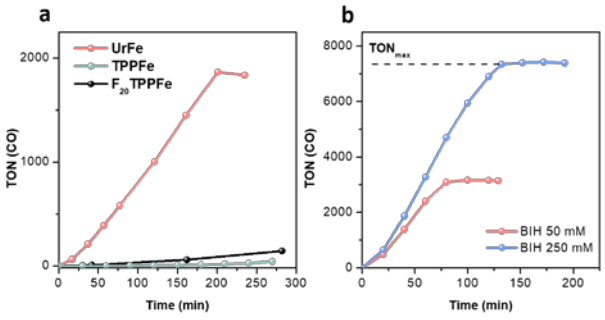

Figure 1 Time evolution of CO produced under **a)** visible light irradiation (λ>405 nm, 100 W m^{-2}) with **TPPFe** (green) **F_{20}TPPFe** (black) or **UrFe** (red) as catalyst with 20 μM concentration; $[Ru(bpy)_3]^{2+}$ photosensitizer 1 mM, BIH sacrificial electron donor 50 mM in CO_2-saturated DMF/H_2O 9:1.**b)** light irradiation with a blue LED (λ_{em}=460 nm 100 W m^{-2}) of **UrFe** as catalyst with 20 μM concentration; $[Ru(bpy)_3]^{2+}$ photosensitizer 1 mM, BIH sacrificial electron donor 50 mM (red) and 250 mM (blue) in CO_2-saturated DMF/H_2O 9:1.

catalytic run performed in presence of a much larger excess of BIH (250 mM) revealed that the reaction can reach an exceptionally high TON of 7271 within 2 hours (Figure 1b and

ACCEPTED MANUSCRIPT - CLEAN COPY

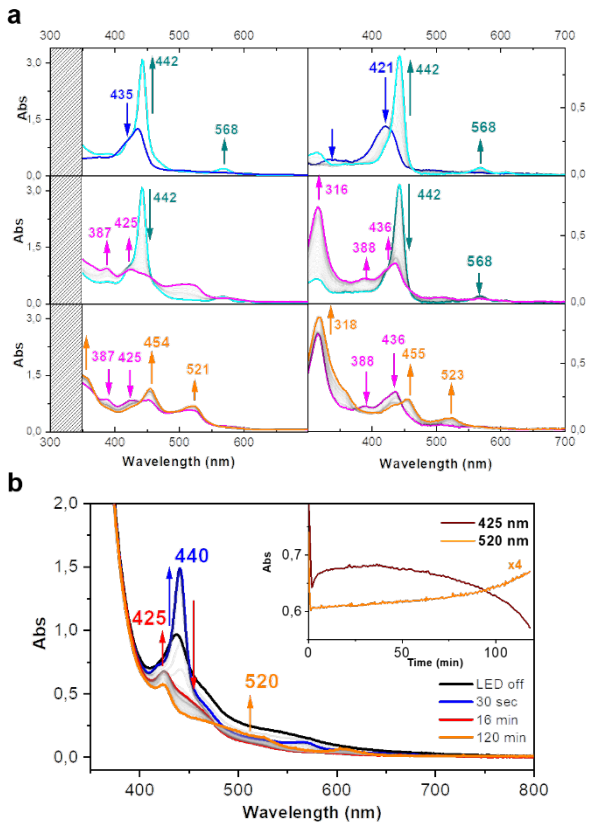

Figure 2. a) Left: UV-vis spectra recorded in photoaccumulation experiment with **UrFe** 10 μM, $[Ru(bpy)_3]^{2+}$ 15 μM, BIH 7 mM in N_2-saturated DMF_{dry} at −35 °C. Top: reference spectra of $\mathbf{UrFe^{III}}$ under Ar and the first spectrum corresponding to $\mathbf{UrFe^{II}}$ reduced in the dark. Middle and bottom: spectral evolution with LED on (λ_{em}=460 nm, 3 W m^{-2}). Right: UV-vis spectral evolution in spectroelectrochemistry experiment with **UrFe** 40 μM in Ar-saturated DMF_{dry}, 0.1 M $TBAPF_6$, at room temperature, Pt Working Electrode, Pt Counter Electrode and Pt pseudo-Reference Electrode; Room Temperature. Top: Fe^{III} to Fe^{II} reduction; Middle: Fe^{II} to Fe^{I} reduction; Bottom: Fe^{I} to Fe^{0} reduction. **b)** UV-vis spectra recorded in photoaccumulation experiment with **UrFe** 5 μM, $[Ru(bpy)_3]^{2+}$ 20 μM, BIH 70 mM in DMF/H_2O 9:1 and 60 mM CO_2. Blue LED (λ_{em} = 460 nm, 70 W m^{-2}), 25°C. Inset: Kinetic profile of Fe^{I} (brown) and Ru^{I} (orange) species.

Table 1b, entry 7). Reinjecting $[Ru(bpy)_3]^{2+}$, CO_2 or a stronger proton source (phenol) into the catalytic system did not restart the catalysis (Figure S4), indicating that the TON obtained is the maximum before deactivation of the catalyst. Using acetonitrile (ACN) water (ACN)/H_2O) as solvent mixture drastically reduced the photocatalytic activity (Figure S5), which is to be linked to the reversibility of the electron donor in ACN/H_2O. When other electron donors with partial reversibility are used, the speed of the reaction is drastically lowered (Table S2, entries 2, 5).

An important increase in the TON was reported in different studies upon lowering the catalyst concentration.[39-43] It was argued that such an enhancement reflects that only a fraction of the catalyst at high concentration was involved in CO_2 reduction while the remaining fraction acted as a reservoir to palliate the progressive deactivation over time. A similar behavior was observed when the concentration of **UrFe** was lowered to 0.2 μM (Table 1, entry 8 Figure S6), yielding a TON as high as 13 300. Accordingly, such a TON can be pinned among the highest observed photocatalytic performances with molecular based catalysts. As a caveat though, the low level of accuracy when measuring small amounts of produced CO and a small photocatalytic activity of the degraded photosensitizer may be of concern at low catalyst loading. Importantly, control experiments in the absence of one component of the reaction *ie*. $[Ru(bpy)_3]^{2+}$, **UrFe**, H_2O, CO_2 and SED, did not show photocatalytic CO production (Table S2 entries 3,4,6). This experiment rules out any participation of the catalyst as an intrinsic chromophore-catalyst system during photocatalysis. In absence of the catalyst, a feeble photocatalytic activity was observed that probably originates from the degradation of the $[Ru(bpy)_3]^{2+}$ photosensitizer.[44] Experiments with ^{13}C labeled CO_2 were performed and confirmed the carbon source of CO (Figure S7).

We then move on to investigate the reaction mechanism under our optimized conditions. First, to identify which component was governing the reaction rate, the photocatalytic reaction was performed with different light intensity, CO_2 concentration and acid strength. As mentioned above, switching from white to blue LED increases the reaction rate. However, further increase of the blue light intensity does not dramatically increases the rate of CO production, indicating that after optimization, the light-driven concentration of the reductant can be considered as constant (Figure S8). However, a clear first order dependency of reaction rate on the substrate (CO_2) concentration can be observed (Figure S9). This indicates that the interaction of CO_2 with an active form the catalyst is involved in the RDS. In our previous studies, we found that the protonation step was the RDS in the electrochemical reduction of CO_2 by **UrFe** with a major kinetic isotope effect (KIE = 5.77).[37] In the case of light-induced catalysis, a much smaller KIE of 1.17 was found (Figure S10) that tends to support that the protonation step has only a limited contribution to the overall rate of the reaction. Furthermore, when proton donors with different pK_a were employed, only a little influence of the proton donor on the catalytic activity was observed (Figure S11).

With the first hint on CO_2 implication in the RDS of the reaction, we sought further confirmation by monitoring the UV-vis spectral evolution during the catalytic reaction. But prior to that, we had to gather the spectral signatures of **UrFe** in different the oxidation states and conditions. To do so, we performed photo-accumulation experiments to generate these species spectral features using $[Ru(bpy)_3]^{2+}$/BIH as photosensitizer/electron donor couple in the absence of the substrate and water. As depicted in Figure 2a, UV-vis spectra show a rapid shift (within the mixing time) of the **UrFe** Soret band from 435 nm to a new band at 442 nm upon mixing of **UrFe** (10μM) with $[Ru(bpy)_3]^{2+}$ (15 μM) and BIH (7 mM) in nitrogen-saturated DMF solution in the dark. The same process was observed when excluding $[Ru(bpy)_3]^{2+}$ (Figure S13). The spectral features are attributed to the formation of $\mathbf{UrFe^{II}}$ as they are consistent with those identified by chemical reduction of $\mathbf{UrFe^{III}}$ using zinc amalgam (Figure S14) as well as by electrochemical reduction (Figure 2a, top right). Under blue light (460nm LED, 3 W m^{-2}) irradiation, the excited state $^*[Ru(bpy)_3]^{2+}$ is reductively quenched by BIH to form the highly reducing $[Ru^{II}(bpy)_2(bpy^{\bullet-})]^+$ species abbreviated here as the formal Ru^{I} species ($E(Ru^{II/I})$ = -1.05 V *vs.* NHE) that in turn drives the formation of $\mathbf{UrFe^{I}}$ ($E(Fe^{II/I})$ = -0.63 V *vs.* NHE) displaying absorption bands at 387 and 425 nm (Figure 2a, center left).[26-27] Although the third reduction is slightly thermodynamically uphill ($E(Fe^{I/0})$ = -1.12 V *vs.* NHE) (Table S1), when present in excess,

ACCEPTED MANUSCRIPT - CLEAN COPY

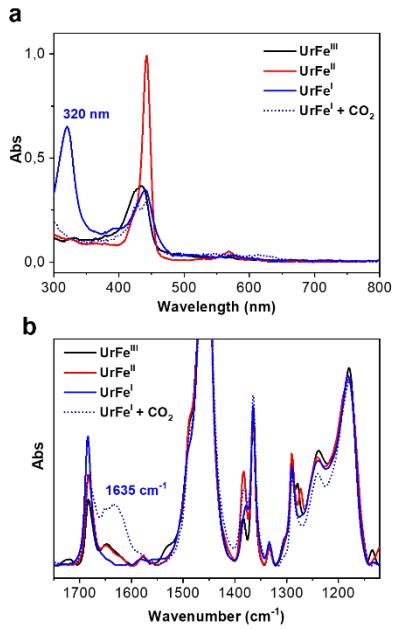

Figure 3. CO_2 influence on the **UrFe^{I}** reduced states monitored by spectro-electrochemistry in the UV-visible region in DMF (**a**) and infrared region in THF (**b**). **UrFe^{III}** (black), **UrFe^{II}** (red) and **UrFe^{I}** state (blue solid line) in Ar and comparison of **UrFe^{I}** in presence of CO_2 (blue dashed line).

Ru^{I} can also promote the formation of **UrFe^{0}** (454 and 521 nm) oxidation state at longer reaction time (Figure 2a, bottom left). The nature of these two last species was confirmed using UV-vis spectro-electrochemistry (Figure 2a, right). Indeed, starting from **UrFe** controlled potential electrolysis performed successively at the potentials corresponding to the $Fe^{III/II}$, $Fe^{II/I}$ and $Fe^{I/0}$ redox couples, show a trend of changes similar to those observed in the photo-accumulation experiment with only a few nm shifts in the absorption bands, due probably to the presence or absence of the electrolyte between the two experiments. The presence of isosbestic points and the full recovery of the **UrFe** Soret band when the reaction mixture was exposed to air (Figure S15) indicate the catalyst does not undergo any significant degradation under these experimental conditions.

In the next step, we monitored the catalytic reaction in presence of a limited amount (60 mM) of the substrate (Figure 2b) and in presence of H_2O as proton source. After a fast transition (30 s) where **UrFe^{II}** accumulates in the reaction mixture as indicated by the strong Soret band at 440 nm, the reaction reaches its steady state with a band at 425 that persists until the total consumption of the substrate. The end of the catalytic reaction is marked by the appearance of the band at 520 nm due to the accumulation of $[Ru(bpy)_3]^{+}$ after depletion of the substrate. As we have determined that CO_2 binding is involved in the RDS, we were expecting to observe the spectral features of **UrFe^{0},** commonly considered to be the active species that activate CO_2. Surprisingly, we observed a steady state with a marked absorption band at 425 nm, characteristic of an **UrFe^{I}** species. This unexpected observation suggests that the CO_2 binding with the catalyst at Fe^{I} oxidation state is the RDS. To investigate this hypothesis, the UV-vis of the electrochemically generated **UrFe^{II}** and **UrFe^{I}** were recorded under argon and CO_2 atmosphere (Figure 3a and S17). As expected, no significant change is apparent when comparing spectra for **UrFe^{II}** in an argon or a CO_2 atmosphere (Figure S17). However, for **UrFe^{I}** under CO_2 we observed the disappearance of the absorption band at 320 nm together with the splitting of the Soret band at 427 and 441 nm (Figure 3a, S17 and S18). Of note, due to the prominent absorption bands of the BIH in the UV region, we could not monitor the spectral change of the catalyst in this region. Further evidence comes from infrared spectro-electrochemistry experiments (Figure 3b, S22) showing that at a potential window where **UrFe^{I}** can be generated, a new broad band at 1635 cm^{-1} appears in presence of CO_2. This particular vibrational signature was detected and attributed to the CO_2 binding in bimetallic NiFe inorganic models of CODH and in a molecular dinuclear Co^{I} complex.[45-46] Hence, this preamble interaction of CO_2 at the Fe^{I} state set the stage for an alternate mechanistic pathway, a premiere that differs from the current electrocatalytic route through the comparatively slow and stepwise e^{-} delivery occurring from the reducing Ru^{I} species. As for the **F$_{20}$TPPFe** catalyst, no clear signature of the steady state could be obtained, entertaining the idea of a probable multibranched photocatalytic process. However, electrochemical generation of **F$_{20}$TPPFe^{I}** in the presence of CO_2 did not induce any spectral changes (Figure S18). This suggests that the Fe^{I}-CO_2 adduct does not form in this oxidation state and that a more reduced Fe^{0} needs to be reached before activating CO_2. Another difference with **UrFe** is the linear dependency of the TOF on the light intensity (Fig S8) we observed. It is thus proposed that the RDS in the case of **F$_{20}$TPPFe** may involve this second photoinduced electron transfer process, in agreement with the thermodynamics of such an endergonic process (+70 mV *ie* +1.6 kcal/mol, Fig S1, Table S2).

DFT calculations were performed to interrogate the possible interaction of the Fe^{I} species with CO_2 for both the **UrFe^{I}** and **F$_{20}$TPPFe^{I}** species (Figure S23-S24 and Table S3). With the **UrFe^{I}** model, a CO_2 adduct was localized only 0.78 kcal/mol higher than the dissociated pair. This energy difference corresponds to an association constant of ca. 1 M^{-1}, too small to be evidenced at the $UrFe^{II/I}$ redox wave by cyclic voltammetry. In contrast, the **F$_{20}$TPPFe^{I}-CO$_2$** species was disfavored by 10.46 kcal/mol thus rendering CO_2 coordination at the Fe^{I} species quite unlikely (k_A = 9 10^{-8} M^{-1}). The superior binding affinity of **UrFe^{I}** is

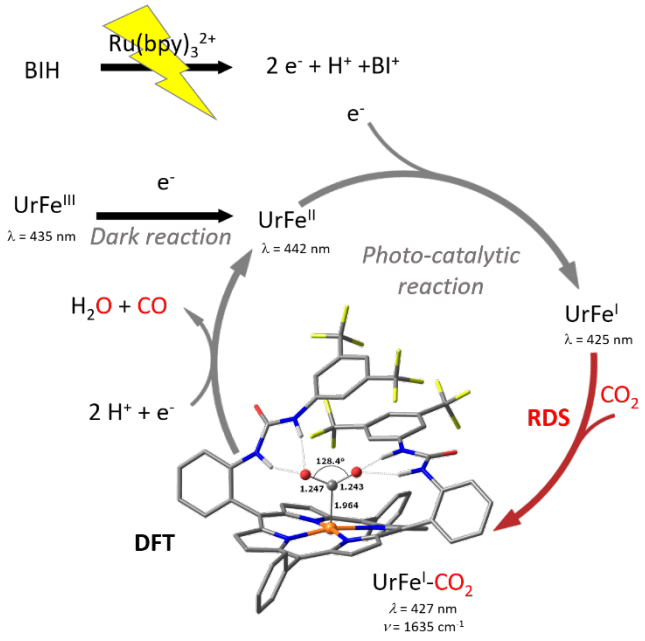

Scheme 1. Proposed mechanism for the light-induced CO_2 reduction to CO with **UrFe** with the species characterized.

ACCEPTED MANUSCRIPT - CLEAN COPY

imputable to the presence of the two urea arms that position the CO_2 in a η^1 coordination mode (Fe-C=1.964 Å, OCO=128.4°, av. C-O=1.246 Å). We were rather surprised to note that this coordination results in a substantial activation of the substrate. Accordingly, the computed geometry, reveals that the bound CO_2 closely resembles a $CO_2^{\bullet-}$ free radical (OCO=133.6°, C-O=1.244 Å) with a charge of -0.67 transferred from the **UrFe^{I}** moiety. Hence this interaction can be seen as a partial charge transfer from the **UrFe^{I}** to CO_2 that would lead to a limit formula of [**UrFe^{II}-$CO_2^{\bullet-}$**]. However, we opted for the writing as a formal [**UrFe^{I}-CO_2]** adduct. As observed experimentally, the vibrational spectra of model **UrFe^{II}** and **UrFe^{I}** our calculations showed only subtle differences in the 1100-1750 cm^{-1} window. However, marked differences were observed for [**UrFe^{I}-CO_2]**. In particular, two vibration modes were identified at 1627 and 1657 cm^{-1} involving an asymmetrical stretching of the bound CO_2 (Fig S27). This result resonates with the experimental vibrational band observed at 1635 cm^{-1}. It is worth noting that a recent report from A. Dey *and coll.* also described the activation of CO_2 at the Fe^{I} oxidation state of a modified Iron-chlorin catalyst that catalyzes the selective reduction of CO_2 to formic acid.[47]

Putting together all the experimental and theoretical findings in this study, we can propose a mechanism for the photocatalytic reduction of CO_2 by **UrFe** as depicted in Scheme 1. The entry of the **UrFe^{II}** species in the cycle occurs in the dark by the reduction of **UrFe^{III}** with BIH. The first photophysical event concerns the reductive quenching of the excited state of the photosensitizer to form the reducing $[Ru(bpy)_3]^+$ that triggers an electron transfer to yield **UrFe^{I}** intermediate. UV-vis monitoring of the reaction revealed this latter to be the steady-state that precedes the rate determining step of the catalytic reaction i.e. the CO_2 binding to **UrFe^{I}** forming the formal [**UrFe^{I}-CO_2]** adduct. Concerning the intervention of the proton in the catalytic cycle, the small KIE found, cannot guarantee its involvement in the RDS. The consequent steps involve the input of another electron and two protons to release CO and a water molecule as products and regenerating **UrFe^{II}**. Another important finding is that at no point we have detected the presence of an Fe^{II}-CO species that is usually considered as the ending point of the photocatalytic or electrocatalytic cycle for the CO_2 to CO conversion. We recall that the iron^{II}-carbonyl intermediate was proposed to accumulate for further reduction to methane under irradiation at higher wavelength than 420 nm.[48] Irradiating a chemically prepared **[UrFe^{II}-CO]** at 460 nm confirms the rapid expulsion of the bound CO (Figure S20).

In conclusion, we found that the light-driven CO_2 reduction using **UrFe** catalyst lead to a multifold increase in TON and TOF compared to both non-substituted **TPPFe** and fluorinated **F_{20}TPPFe**, reaching one of the highest values in molecular photocatalysis and importantly with water as proton source. In contrast to the classic photocatalytic scheme where Fe^0 is argued to be the species to react with CO_2, we evidenced that the RDS herein resides in the formation of the [**UrFe^{I}-CO_2]** adduct. The added urea functionality plays an important role in the binding and activation of CO_2 at the Fe^{I} state enabling the faster photocatalytic conversion. Further work is in progress to better characterize and follow the fate of the [**UrFe^{I}-CO_2]** adduct and the deactivation route of the catalyst.

Acknowledgements

This work has been supported by the French National Research Agency (LOCO, grant N°: ANR-19-CE05-0020-02 and LABEX CHARMMMAT, grant N°: ANR-11-LABX-0039). DFT calculations were performed using HPC resources from GENCI (grant A0070810977). We thank CNRS, CEA Saclay, ICMMO and University Paris-Saclay for the financial support. A. A. thanks the Institut Universitaire de France for support.

Keywords: Iron • Porphyrins • Carbon dioxide • Photo-reduction • Mechanism

[1] T. Cardona, A. Sedoud, N. Cox, A. W. Rutherford, *Biochim. Biophys. Acta* **2012**, *1817*, 26-43.
[2] H. Dau, I. Zaharieva, *Acc. Chem. Res.* **2009**, *42*, 1861-1870.
[3] V. Balzani, A. Credi, M. Venturi, *ChemSusChem* **2008**, *1*, 26-58.
[4] J. Bian, J. Feng, Z. Zhang, J. Sun, M. Chu, L. Sun, X. Li, D. Tang, L. Jing, *Chem. Commun.* **2020**.
[5] S. Kreft, R. Schoch, J. Schneidewind, J. Rabeah, E. V. Kondratenko, V. A. Kondratenko, H. Junge, M. Bauer, S. Wohlrab, M. Beller, *Chem* **2019**, *5*, 1818-1833.
[6] M. Schreier, L. Curvat, F. Giordano, L. Steier, A. Abate, S. M. Zakeeruddin, J. Luo, M. T. Mayer, M. Gratzel, *Nat Commun* **2015**, *6*, 7326.
[7] H. Park, H. H. Ou, A. J. Colussi, M. R. Hoffmann, *J. Phys. Chem. A* **2015**, *119*, 4658-4666.
[8] H. S. Jeon, J. H. Koh, S. J. Park, M. S. Jee, D.-H. Ko, Y. J. Hwang, B. K. Min, *J Mater Chem A* **2015**, *3*, 5835-5842.
[9] T. Arai, S. Sato, T. Morikawa, *Energy Environ. Sci.* **2015**, *8*, 1998-2002.
[10] S. Sato, T. Arai, T. Morikawa, K. Uemura, T. M. Suzuki, H. Tanaka, T. Kajino, *J. Am. Chem. Soc.* **2011**, *133*, 15240-15243.
[11] X. Liu, S. Inagaki, J. Gong, *Angew. Chem. Int. Ed.* **2016**, *55*, 14924-14950.
[12] J. Albero, Y. Peng, H. García, *ACS Catal.* **2020**, *10*, 5734-5749.
[13] N. Serpone, A. V. Emeline, *J. Phys. Chem. Lett.* **2012**, *3*, 673-677.
[14] A. Rosas-Hernández, C. Steinlechner, H. Junge, M. Beller, *Top. Curr. Chem.* **2017**, *376*, 1.
[15] A. M. Appel, J. E. Bercaw, A. B. Bocarsly, H. Dobbek, D. L. DuBois, M. Dupuis, J. G. Ferry, E. Fujita, R. Hille, P. J. A. Kenis, C. A. Kerfeld, R. H. Morris, C. H. F. Peden, A. R. Portis, S. W. Ragsdale, T. B. Rauchfuss, J. N. H. Reek, L. C. Seefeldt, R. K. Thauer, G. L. Waldrop, *Chem. Rev.* **2013**, *113*, 6621-6658.
[16] M. Aresta, A. Dibenedetto, A. Angelini, *Chem. Rev.* **2014**, *114*, 1709-1742.
[17] B. Kumar, M. Llorente, J. Froehlich, T. Dang, A. Sathrum, C. P. Kubiak, *Annu. Rev. Phys. Chem.* **2012**, *63*, 541-569.
[18] M. Cokoja, C. Bruckmeier, B. Rieger, W. A. Herrmann, F. E. Kühn, *Angew. Chem. Int. Ed.* **2011**, *50*, 8510-8537.
[19] S. C. Roy, O. K. Varghese, M. Paulose, C. A. Grimes, *ACS Nano* **2010**, *4*, 1259-1278.
[20] S. Amanullah, P. Saha, A. Nayek, M. E. Ahmed, A. Dey, *Chem. Soc. Rev.* **2021**, *50*, 3755-3823.
[21] N. W. Kinzel, C. Werlé, W. Leitner, *Angew. Chem. Int. Ed.* **2021**, *60*, 11628-11686.
[22] F. Franco, C. Rettenmaier, H. S. Jeon, B. Roldan Cuenya, *Chem. Soc. Rev.* **2020**, *49*, 6884-6946.
[23] R. Bonetto, F. Crisanti, A. Sartorel, *ACS Omega* **2020**, *5*, 21309-21319.

[24] R. Francke, B. Schille, M. Roemelt, *Chem. Rev.* **2018**, *118*, 4631-4701.
[25] P. Gotico, Z. Halime, A. Aukauloo, *Dalton Trans.* **2020**, *49*, 2381-2396.
[26] A. W. Nichols, C. W. Machan, *Front Chem* **2019**, *7*, 397.
[27] F. Franco, S. Fernández, J. Lloret-Fillol, *Current Opinion in Electrochemistry* **2019**, *15*, 109-117.
[28] H. Takeda, C. Cometto, O. Ishitani, M. Robert, *ACS Catal.* **2017**, *7*, 70-88.
[29] A. Call, M. Cibian, K. Yamamoto, T. Nakazono, K. Yamauchi, K. Sakai, *ACS Catalysis* **2019**, *9*, 4867-4874.
[30] C. Costentin, S. Drouet, M. Robert, J.-M. Savéant, *Science* **2012**, *338*, 90-94.
[31] J. Bonin, M. Robert, M. Routier, *J. Am. Chem. Soc.* **2014**, *136*, 16768-16771.
[32] C. Romelt, J. Song, M. Tarrago, J. A. Rees, M. van Gastel, T. Weyhermuller, S. DeBeer, E. Bill, F. Neese, S. Ye, *Inorg. Chem.* **2017**, *56*, 4746-4751.
[33] C. Romelt, S. Ye, E. Bill, T. Weyhermuller, M. van Gastel, F. Neese, *Inorg. Chem.* **2018**, *57*, 2141-2148.
[34] A. J. Göttle, M. T. M. Koper, *Journal of the American Chemical Society* **2018**, *140*, 4826-4834.
[35] Y.-Q. Zhang, J.-Y. Chen, P. E. M. Siegbahn, R.-Z. Liao, *ACS Catalysis* **2020**, *10*, 6332-6345.
[36] T. Mashiko, C. A. Reed, K. J. Haller, W. R. Scheidt, *Inorg. Chem.* **1984**, *23*, 3192-3196.
[37] P. Gotico, B. Boitrel, R. Guillot, M. Sircoglou, A. Quaranta, Z. Halime, W. Leibl, A. Aukauloo, *Angew. Chem. Int. Ed.* **2019**, *58*, 4504-4509.
[38] P. Gotico, L. Roupnel, R. Guillot, M. Sircoglou, W. Leibl, Z. Halime, A. Aukauloo, *Angew. Chem. Int. Ed. Engl.* **2020**, *59*, 22451-22455.
[39] S. L.-F. Chan, T. L. Lam, C. Yang, S.-C. Yan, N. M. Cheng, *Chem. Commun.* **2015**, *51*, 7799-7801.
[40] V. S. Thoi, N. Kornienko, C. G. Margarit, P. Yang, C. J. Chang, *J. Am. Chem. Soc.* **2013**, *135*, 14413-14424.
[41] T. Ouyang, H.-H. Huang, J.-W. Wang, D.-C. Zhong, T.-B. Lu, *Angew. Chem. Int. Ed.* **2017**, *56*, 738-743.
[42] D. Hong, Y. Tsukakoshi, H. Kotani, T. Ishizuka, T. Kojima, *J. Am. Chem. Soc.* **2017**, *139*, 6538-6541.
[43] H. Yuan, B. Cheng, J. Lei, L. Jiang, Z. Han, *Nat Commun* **2021**, *12*, 1835.
[44] J. Hawecker, J.-M. Lehn, R. Ziessel, *J. Chem. Soc., Chem. Commun.* **1985**, 56-58.
[45] Z. Guo, G. Chen, C. Cometto, B. Ma, H. Zhao, T. Groizard, L. Chen, H. Fan, W.-L. Man, S.-M. Yiu, K.-C. Lau, T.-C. Lau, M. Robert, *Nature Catalysis* **2019**, *2*, 801-808.
[46] J.-E. Lee, A. Yamaguchi, H. Ooka, T. Kazami, M. Miyauchi, N. Kitadai, R. Nakamura, *Chem. Commun.* **2021**, *57*, 3267-3270.
[47] S. Amanullah, P. Saha, A. Dey, *J. Am. Chem. Soc.* **2021**, *143*, 13579-13592.
[48] H. Rao, L. C. Schmidt, J. Bonin, M. Robert, *Nature* **2017**, *548*, 74-77.

ACCEPTED MANUSCRIPT - CLEAN COPY

Entry for the Table of Contents

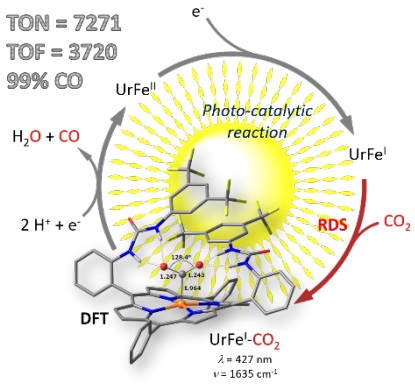

The exceptionally high performance for CO_2-to-CO photocatalytic reduction displayed by an Iron-porphyrin bearing urea groups in the second coordination sphere is the result of the interaction CO_2 with the catalyst prior the occurrence of the second electron uptake in the catalytic cycle.